Magnetic Hysteresis Under Compressive Stress: A Multiscale-Jiles–Atherton Approach

L. Bernard[1], B. J. Mailhé[1], S. L.Ávila[2], L. Daniel[3], N. J. Batistela[1], and N. Sadowski[1]

[1]GRUCAD, EEL, CTC, Federal University of Santa Catarina (UFSC), Florianópolis 88040-900, Brazil
[2]PECCE/IFSC, Federal Institute of Santa Catarina, Florianópolis 88020-300, Brazil
[3]Group of Electrical Engineering-Paris (GeePs), UMR CNRS 8507, CentraleSupélec, Univ. Paris-Sud, Université Paris-Saclay, Sorbonne Université, 91192 Gif-sur-Yvette, France

Based on multiscale modeling of the anhysteretic magnetization considering mechanical stress and crystallographic texture effects, an extension of the Jiles–Atherton (J-A) hysteresis model is proposed. The magnetization and the volume fractions given by the multiscale approach are advantageously used in the J-A model to modify the anhysteretic magnetization and the pinning parameter. The parameters of the proposed model are identified in order to fit with the characterization results under compressive stress using two sets of experimental data. Using the same optimized parameters, the model is tested for the representation of loops under other stress conditions to evaluate its prediction capabilities.

Index Terms— **Jiles–Atherton (J-A) model, magnetic hysteresis, magneto-elasticity, multiscale model.**

I. Introduction

MECHANICAL stress has a strong effect on magnetic hysteresis. In particular, the shape and area (energetic loss density) of the hysteresis loops are modified by relatively low compressive stresses. Usual electrical steel may suffer a power loss increase of 50% to 500% under a compressive stress of 50 MPa [1], depending on the applied magnetic induction. Different approaches have already been proposed to represent this phenomenon using modified Jiles–Atherton (J-A) [2] or hysteretic multiscale [3] models. An intermediate approach consists of the association of a vector J-A magnetic hysteresis model with an anhysteretic simplified multiscale model (SMSM). The aim is to obtain a fully vectorial model with a reasonable computational evaluation time, so that it can be used for device simulations [4]. SMSMs can be extended [5] to allow representing some phenomena induced by the combination of crystal anisotropy and crystallographic texture. A variable J-A k pinning parameter (depending on the domain configuration) is proposed in order to fit the shape of the hysteresis loops under compressive stress. The model parameters are identified by optimization using two sets of characterization results under mechanical stress obtained from a modified single-sheet tester [6] and an external reference [7], for Fe-3% Si electrical steel sheets.

II. SMSM With Crystallographic Texture

Polycrystalline magnetic materials consist of a set of grains with different orientations. The SMSM evaluates the magnetization assuming that the applied magnetic field ($\vec{H}$) and mechanical stress ($\boldsymbol{\sigma}$) are homogeneous. Each grain is made of a set of magnetic domain families characterized by their orientation $\vec{\alpha}$ and volume fraction $f_\alpha d\alpha$. The magnetization of one grain is then

$$\vec{M}_g = M_s \int f_\alpha \, \vec{\alpha} \, d\alpha \tag{1}$$

where M_s is the saturation magnetization and the integral is evaluated on the set of possible orientations (652 orientations are used for numerical integration). The volume fractions can be calculated through a Boltzmann statistics considering

$$f_\alpha = \exp(-A_s W_\alpha) / \int \exp(-A_s W_\alpha) d\alpha \tag{2}$$

where A_s is a material constant and W_α is the potential energy of each domain family and is the sum of magnetostatic, magneto-elastic, and anisotropy components

$$W_\alpha^{\text{mag}} = -\mu_0 \vec{H} \cdot \vec{M}_\alpha \tag{3}$$

$$W_\alpha^{\text{el}} = -\boldsymbol{\sigma} : \boldsymbol{\varepsilon}_\alpha^{\mu} \tag{4}$$

$$W_\alpha^{\text{an}} = K_1\left(\alpha_1^2\alpha_2^2 + \alpha_2^2\alpha_3^2 + \alpha_3^2\alpha_1^2\right). \tag{5}$$

The unit vector $\vec{\alpha} = (\alpha_1, \alpha_2, \alpha_3)$ represents the direction of a domain family. The associated magnetization and magnetostriction strain are

$$\vec{M}_\alpha = M_s \vec{\alpha} \tag{6}$$

$$\boldsymbol{\varepsilon}_\alpha^{\mu} = \frac{3}{2}\begin{bmatrix} \lambda_{100}\left(\alpha_1^2 - \frac{1}{3}\right) & \lambda_{111}\alpha_1\alpha_2 & \lambda_{111}\alpha_1\alpha_3 \\ \lambda_{111}\alpha_2\alpha_1 & \lambda_{100}\left(\alpha_2^2 - \frac{1}{3}\right) & \lambda_{111}\alpha_2\alpha_3 \\ \lambda_{111}\alpha_3\alpha_1 & \lambda_{111}\alpha_3\alpha_2 & \lambda_{100}\left(\alpha_3^2 - \frac{1}{3}\right) \end{bmatrix}. \tag{7}$$

These expressions of anisotropic energy (5) and magnetostriction strain (7) are for cubic crystals. The anisotropy constant K_1, the saturation magnetization M_s, and the saturation magnetostriction constants λ_{100} and λ_{111} are the parameters defined at the material single crystal scale. A_s is a macroscopic parameter related to the initial slope of the magnetization

Manuscript received August 15, 2019; revised October 3, 2019; accepted October 4, 2019. Date of current version January 20, 2020. Corresponding author: L. Bernard (e-mail: laurent.bernard@ufsc.br).

Color versions of one or more of the figures in this article are available online at http://ieeexplore.ieee.org.

Digital Object Identifier 10.1109/TMAG.2019.2946115

TABLE I
PARAMETERS OF THE SMSM FROM [3]

$A_s(m^3/J)$	$M_s(A/m)$	λ_{100}	λ_{111}	$K_1(kJ/m^3)$
$3 \cdot 10^{-3}$	$1.6 \cdot 10^6$	$23 \cdot 10^{-6}$	$-4.5 \cdot 10^{-6}$	38

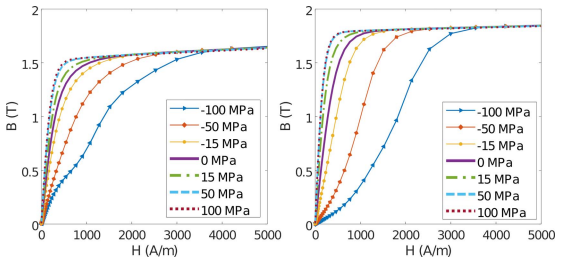

Fig. 1. Anhysteretic magnetization for different values of stress (uniaxial configuration) for the axial ⟨111⟩ (left) and ⟨100⟩ (right) fibers.

curve [3]. From the magnetization $\vec{M}_g$, the macroscopic behavior is calculated by a weighted sum over grain orientations (defined by the crystallographic texture)

$$\vec{M} = \sum_g f_g \vec{M}_g \tag{8}$$

where f_g represents the proportion of each grain orientation in the material.

III. Crystallographic Texture Effects

Reference values of the parameters associated with single crystals can be found in the literature for various ferromagnetic materials. Parameter A_s can be evaluated from a simple macroscopic magnetic characterization without mechanical stress. Information about the crystallographic texture of the material should also be known in order to define a relevant set of grain orientations for the SMSM with crystallographic texture. This information is rarely available together with the magnetoelastic material characterization of the laminated electric steel. Here, we use the parameters of Table I given in [3] for a Fe-3%Si material. Pole figures presented in [3] show a crystallographic texture close to the one of a ⟨111⟩ axial fiber with its axis perpendicular to the sheet plane [5]. To represent this material, a reduced set of four grains is used. The grain orientations are obtained starting from a crystal with a [111] direction perpendicular to the sheet plane and applying rotations, with respect to this axis, of angles uniformly distributed between 0 and $2\pi/3$ (because of the periodicity of this configuration). This completes the definition of the SMSM for this material. For comparison and in order to highlight texture-related effects, we consider also another possible crystallographic texture, corresponding to a ⟨100⟩ axial fiber. In this case, the set of four grains is obtained starting from a crystal with a [100] direction perpendicular to the sheet plane and applying rotations, with respect to this axis, between 0 and $\pi/2$. The magnetization curves for the two types of fiber are shown in Fig. 1 for a uniaxial configuration (uniaxial stress along the magnetic field direction) with different values of mechanical stress.

The results show various characteristics induced by the combination of strong crystal anisotropy and crystallographic texture. In particular, the inflections appearing on the curve under compressive stress (−100 MPa) strongly depend on the crystallographic texture. Compressive stress significantly deteriorates the magnetic properties in both the cases. However, while this effect is especially significant at low magnetic field for the ⟨100⟩ axial fiber, it mainly appears for intermediate magnetic field intensity for the ⟨111⟩ axial fiber. Another considerable difference is visible when reaching saturation. In both the cases, the material remains relatively far from technical saturation ($\mu_0 M_s = 2T$) for the chosen values of applied field, but for the ⟨100⟩ axial fiber, the "knee" region is reached with higher induction and lower magnetic field than the ⟨111⟩ axial fiber. Finally, it can be noted that tensile stress improves the magnetic properties in both the cases in a rather similar way, and this effect saturates for values of stress above 50 MPa. Experimental results [3] demonstrate that the effect of tensile stress should saturate more rapidly and then deteriorate the magnetic properties. This phenomenon cannot be reproduced by the SMSM model (in more complex multiscale approaches, this effect can be accounted for introducing a demagnetizing field depending on the domain configuration [3]).

IV. Association With J-A Model

The vector extension of the J-A model [8] is defined by the magnetization increment, which can be expressed as

$$d\vec{M}_{hys} = \boldsymbol{\chi}_f d\vec{H}_e + c\, d\vec{M}. \tag{9}$$

The effective magnetic field is $\vec{H}_e = \vec{H} + \beta \vec{M}_{hys}$, and $\vec{M}$ is an anhysteretic component function of $\vec{H}_e$. If $\vec{\chi}_f . d\vec{H}_e \leq 0$, $\boldsymbol{\chi}_f$ is the null tensor; otherwise, $\boldsymbol{\chi}_f = \left|\vec{\chi}_f\right|^{-1} \vec{\chi}_f \otimes \vec{\chi}_f$ with $\vec{\chi}_f = (1/k)(\vec{M} - \vec{M}_{hys})$. (β, c, k) is the set of J-A parameters. The anhysteretic magnetization is here determined by the model presented in Section II. As a consequence, the effect of mechanical stress and crystallographic texture on the anhysteretic behavior is considered. However, in order to represent the variations in the hysteresis loop width and losses under stress, it is also necessary to consider the variations of the J-A model parameters. In the original J-A approach, the value of the pinning parameter k, strongly related to hysteresis losses, is expected to change with magnetization or magnetic field. The method by which this parameter changes must be determined experimentally for each material. In a magneto-elastic context, the value of k may also change with mechanical stress. Both these influences can be retrieved from the information contained in the domain configuration of the material. Following [4], we propose to quantify the degree of compatibility between the domain configuration and the magnetization change by

$$\gamma = \sum_g f_g \gamma_g = \sum_g f_g \int f_\alpha |\vec{\alpha} \cdot \vec{\tau}| d\alpha \tag{10}$$

where $\vec{\tau}$ is a unit vector tangent to the trajectory described by magnetization ($\vec{M}$). This synthetic quantity γ depends on the domain volume fractions ($f_\alpha d\alpha$). The pinning parameter k is assumed to depend on γ. The macroscopic phenomenology

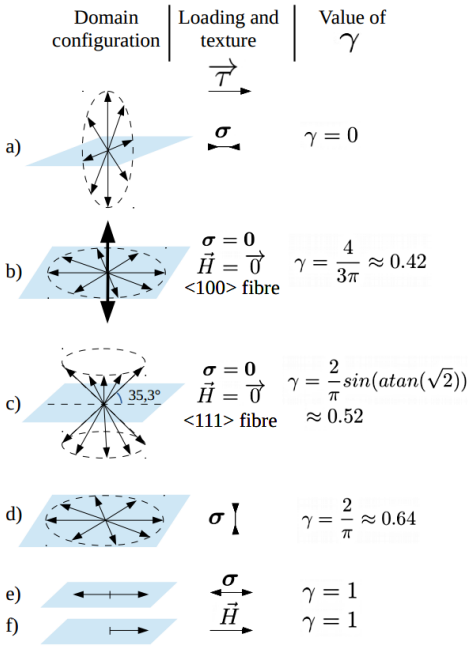

Fig. 2. Values of γ for different domain configurations.

foreseen here [1] is that the higher this degree of compatibility, the lower the losses associated with the magnetization increment.

We may examine some specific cases for γ, summarized in Fig. 2 (cases are ordered by increasing γ). The laminated material is considered with the magnetization increment direction $\vec{\tau}$ in the sheet plane. We consider first Cases b) and c) where no stress and no field are applied: there are only six domain families for each grain (corresponding to the easy directions). For a $\langle 100 \rangle$ axial fiber, noting θ the angle between $\vec{\tau}$ and an easy magnetizing direction [100] for one grain (g), we have $\gamma_g = 2(|\cos(\theta)| + |\sin(\theta)|)/6$. Then, $\gamma = 2/\pi \int_0^{\pi/2} \gamma_g(\theta) d\theta = 4/(3\pi)$ [Fig. 2(b)]. For a $\langle 111 \rangle$ axial fiber, all the [100] directions make an angle of $\text{atan}(\sqrt{2}) \approx 54,7°$ with respect to the direction normal to the sheet. Then, $\gamma = 2/\pi \int_0^{\pi/2} \cos(\theta)\sin(\text{atan}(\sqrt{2}))d\theta = 2/\pi \sin(\text{atan}(\sqrt{2}))$ [Fig. 2(c).

Then, we consider, in Cases a) and d), a material with isotropic domain magnetostriction, on which a strong compressive stress is applied in a direction making an angle ξ with $\vec{\tau}$. The domains may have any orientation in the plane perpendicular to the stress direction and then $\gamma = 2/\pi \sin(\xi)$. In particular, when compressive stress is parallel to $\vec{\tau}$, $\gamma = 0$, and when compressive stress is perpendicular to $\vec{\tau}$, $\gamma = 2/\pi$ [Fig. 2(a) and (d)]. Finally, when a strong tensile stress is applied parallel to $\vec{\tau}$ (two-domain configuration) or when the material is magnetically saturated in the $\vec{\tau}$-direction (one-domain configuration), we have $\gamma = 1$ [Fig. 2 (e) and (f)].

From Fig. 2, it can be seen how γ increases as the domain configuration becomes more favorable with respect to the magnetization increment direction. The chosen parameter γ makes no difference between configurations (e) and (f) despite the fact that magnetization processes from these configurations are different. However, in practice, variations in parameter k appear mainly for small values of γ, far from these configurations.

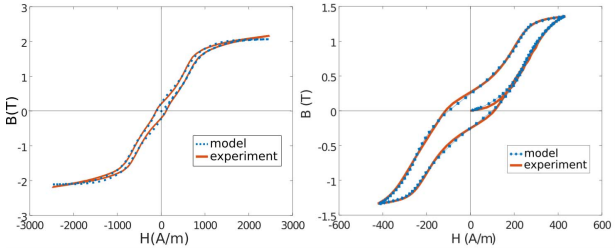

Fig. 3. Hysteresis loops for the optimized model and experiments from references [7] under −35 MPa (left) and [6] under −21.4 MPa (right).

TABLE II
OPTIMIZATION PARAMETERS FOR REFERENCE [7]

Parameter	Value	Range	Unit
a	116.3	1, 500	A/m
M_s	2.12	1.5, 2.5	$10^6 A/m$
β	$1.45 \cdot 10^{-4}$	0, 10^{-3}	-
c	0.380	0.05, 0.9	-
K_1	144.5	1, 200	kJ/m^3
λ_{100}	53.1	5, 100	ppm
λ_{111}	−10.0	−30, −1	ppm
$k(\gamma)$	(599; 138; 88; 81; 107)	2, 2500	A/m

TABLE III
OPTIMIZATION PARAMETERS FOR REFERENCE [6]

Parameter	Value	Range	Unit
a	51.9	1, 100	A/m
M_s	1.36	1, 2	MA/m
β	$1.37 \cdot 10^{-4}$	10^{-5}, 10^{-3}	-
c	0.395	0.005, 0.9	-
K_1	3.14	1, 100	kJ/mˆ3
λ_{100}	16.2	5, 50	ppm
λ_{111}	−12.5	−20, −1	ppm
$k(\gamma)$	(227; 140; 59; 94; 100)	10, 500	A/m

V. OPTIMIZATION OF MODEL PARAMETERS

The SMSM and the J-A model are based on a physical representation of magnetization processes and some strong simplifying assumptions. To fit a particular material hysteresis loop, an optimization can be applied to all the model parameters, even those that are theoretically given by the crystal characteristics (such as M_s, λ_{100}, λ_{111}, and K_1). The hysteresis loops for the non-oriented Fe-3%Si-laminated material from references [7] and [6], under a compressive stress of −35 and −21.4 MPa, respectively, are considered. For both the references, neither the crystallographic texture information nor the anhysteretic behavior is available. Looking at the experimental hysteresis loops (Fig. 3) and the modeled anhysteretic behavior (Fig. 1), one might guess that the material of reference [7] is similar to a $\langle 111 \rangle$ axial fiber, while the material in reference [6] is similar to a $\langle 100 \rangle$ axial fiber. From this observation, we choose to fix the selected simplified crystallographic texture for each material. A genetic algorithm [9] is used to fit the hysteresis loop under compressive stress considering the rms error between the model and experimental results as an objective function. Parameter k is considered as a piecewise linear function of γ using five reference values of γ (0; 0.25; 0.5; 0.75; 1). All the parameters are optimized using predefined search ranges (Tables II and III).

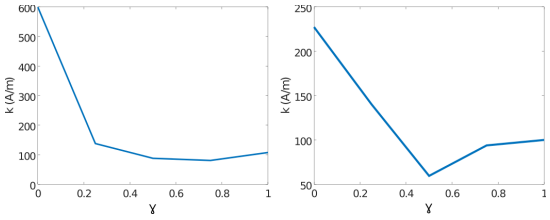

Fig. 4. Optimized $k(\gamma)$ functions for references [7] (left) and [6] (right).

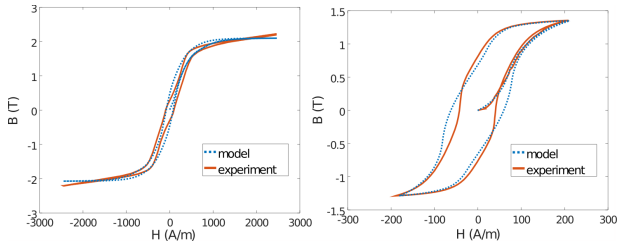

Fig. 5. Hysteresis loops for the optimized model and experiments from references [7] under −18 MPa (left) and [6] under −5.4 MPa (right).

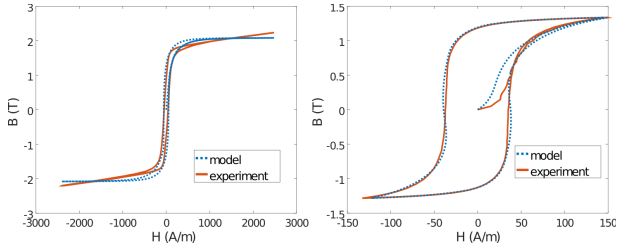

Fig. 6. Hysteresis loops (unstressed) for the optimized model and experiments from references [7] (left) and [6] (right).

For the optimized set of parameters, the model accurately fits with experiment (Fig. 3). For both the materials, the optimized function $k(\gamma)$ decreases significantly between 0 and 0.5 and stabilizes for $\gamma \rangle 0.5$ (Fig. 4). For low values of magnetic field and with the applied compressive stress, the material is in a configuration similar to that shown in Fig. 2(a). When γ is close to 0, the optimized k is relatively high and the resulting hysteresis loop is wider. As γ increases with the magnetic field, and because the experimental loop becomes narrower, k decreases. The values of crystal parameters obtained from optimization differ significantly from the ones of Table I. Such discrepancies are due to the strong simplifications about the physical magnetization processes.

VI. Prediction Capabilities

With the former set of optimized parameters, keeping the maximum induction value constant, experimental and model results are considered for other values of mechanical stress: −18 and 0 MPa for reference [7] and −5.4 and 0 MPa for reference [6] (see Figs. 5 and 6). The model follows correctly the steepness of the experimental hysteresis loops, which increases as the compressive stress becomes smaller. However, the specific shape of the loops is not accurately reproduced for the intermediate values of compressive stress (Fig. 5). When no stress is applied (Fig. 6), the hysteresis loops do not present additional inflections and the model fits correctly with experimental results. However, as the loops become steeper, the model may present an unphysical negative differential permeability. This problem is even more significant under tensile stress and turns the model inapplicable with the same set of parameters. Finally, in the case of reference [6], under −5.4 MPa, the compressive stress seems to deteriorate the magnetization mainly for the intermediate values of magnetic field, comparing Fig. 5 (right) with the unstressed results in Fig. 6 (right). This suggests that the choice of a simplified ⟨100⟩ axial fiber texture for this material, which is well adapted for the representation of the loop under −21.4 MPa, might not be the best one. At −5.4 MPa, the shape of the hysteresis loop seems to fit better with a ⟨111⟩ axial fiber.

VII. Conclusion

It is shown that the magnetization and the domain volume fractions given by a simplified multiscale approach can be used advantageously to extend the J-A model. This allows representing complex hysteresis loop shapes. The anhysteretic curve presents inflections due to the crystallographic texture effects, and the width of the loop varies with the compatibility between the domain configuration and the magnetization increment direction. This compatibility is quantified through the proposed parameter γ. The model has intermediate computational cost compared with other existing models and can be applied to device simulations [5]. Because of the lack of crystallographic texture and anhysteretic information, the choice of the set of grain orientations is based on the shape of the hysteresis loop under stress and the corresponding modeled anhysteretic behavior. The simplified crystallographic texture could be improved to enhance the predictive capabilities of the model. The association of two axial fibers will be analyzed in future works.

Acknowledgment

This work was supported in part by CNPq and in part by CAPES/COFECUB under Project 88881.191763/2018-01.

References

[1] M. LoBue, C. Sasso, V. Basso, F. Fiorillo, and G. Bertotti, "Power losses and magnetization process in Fe–Si non-oriented steels under tensile and compressive stress," *J. Magn. Magn. Mater.*, vols. 215–216, pp. 124–126, Jun. 2000.

[2] M. J. Sablik, G. Kwun, and G. L. Burkhardt, "Model for the effect of tensile and compressive stress on ferromagnetic hysteresis," *J. Appl. Phys.*, vol. 61, no. 8, pp. 3799–3801, 1987.

[3] L. Daniel, M. Rekik, and O. Hubert, "A multiscale model for magneto-elastic behaviour including hysteresis effects," *Arch. Appl. Mech.*, vol. 84, nos. 9–11, pp. 1307–1323, Oct. 2014.

[4] L. Bernard and L. Daniel, "Effect of stress on magnetic hysteresis losses in a switched reluctance motor: Application to stator and rotor shrink fitting," *IEEE Trans. Magn.*, vol. 51, no. 9, pp. 1–13, Sep. 2015.

[5] L. Bernard, B. J. Mailhé, N. Sadowski, N. J. Batistela, and L. Daniel, "Multiscale approaches for magneto-elasticity in device simulation," *J. Magn. Magn. Mater.*, vol. 487, Oct. 2019, Art. no. 165241.

[6] B. J. Mailhé, "Characterization and modelling of the magnetic behaviour of electrical steel under mechanical stress," Ph.D. dissertation, Dept. Elect. Electron. Eng., Univ. Federal Santa Catarina, Florianópolis, Brazil, 2018.

[7] O. Perevertov, "Influence of the applied elastic tensile and compressive stress on the hysteresis curves of Fe-3%Si non-oriented steel," *J. Magn. Magn. Mater.*, vol. 428, pp. 223–228, Apr. 2017.

[8] A. J. Bergqvist, "A simple vector generalization of the Jiles-Atherton model of hysteresis," *IEEE Trans. Magn.*, vol. 32, no. 5, pp. 4213–4215, Sep. 1996.

[9] J. V. Leite *et al.*, "Real coded genetic algorithm for Jiles-Atherton model parameters identification," *IEEE Trans. Magn.*, vol. 40, no. 2, pp. 888–891, Mar. 2004.